Coarse-grained models of tethers for fast self-assembly simulations

Aaron Santos,[1] Chetana Singh,[1] and Sharon C. Glotzer[1,2,*]
[1]*Department of Chemical Engineering, University of Michigan, Ann Arbor, Michigan 48109-2136, USA*
[2]*Department of Materials Science & Engineering, University of Michigan, Ann Arbor, Michigan 48109-2136, USA*
(Received 12 September 2009; published 8 January 2010)

Long molecular ligands or "tethers" play an important role in the self-assembly of many nanoscale systems. These tethers, whose only interaction may be a hard-core repulsion, contribute significantly to the free energy of the system because of their large conformational entropy. Here, we investigate how simple approximate models can be developed and used to quickly determine the configurations into which tethers will self assemble in nanoscale systems. We derive criteria that determine when these models are expected to be accurate. Finally, we propose a generalized two-body approximation that can be used as a toy model for the self-assembly of tethers in systems of arbitrary geometry and apply this to the self-assembly of self-assembled monolayers on a planar surface. We compare our results to those in the literature obtained via atomistic and dissipative particle dynamics simulations.

DOI: 10.1103/PhysRevE.81.011113 PACS number(s): 05.70.−a, 05.10.−a, 05.65.+b, 81.16.Rf

I. INTRODUCTION

Flexible molecular chains play a large role in the self-assembly of nanoscale systems. Tethered polymers, macromolecular chains attached to a surface by their ends, are particularly interesting in this regard [1]. Self-assembled monolayers (SAMs), formed by the adsorption of organic molecules onto a surface, are one such example of a tethered system. The ability to control the arrangement of molecules in SAMs is highly sought to facilitate the development of biocompatible materials, biosensors, microelectromechanical structures (MEMs), membranes, and molecular electronics [2–4]. Two-component SAMs are particularly interesting in this respect because of their ability to microphase separate into patterns whose geometric properties can be controlled by varying the chain length, chemical functionality of the tail group, and composition [5].

Various methods of modeling systems composed of flexible molecules have been developed including self-consistent field theory (SCFT) [6–11], scaling theories [12,13], multiscale modeling [14–16], and cellular free-volume theory [17]. More recently, focus has shifted to the assembly of tether ligands on nanostructured surfaces, particularly nanoparticles (NP) [5,18–22]. Interest in ligand-shell assembly on NPs stems from the desire to combine the chemical properties of ligands with the unique optical and electronic properties of NPs. Toward this end, researchers have studied the formation of Janus particles [23–32], in which NP surfaces are functionalized with two types of ligands. Combining multiple functionalities may lead to novel advances in biological sensing and catalysis [33]. Recently, the self-assembly of ordered stripelike domains on the surface of spherical nanoparticles was reported [5,21]. This stripe phase and its properties have been studied computationally using both atomistic simulations and dissipative particle dynamics [5,22,34,35]. Results from these simulations demonstrate that the microphase separation is thermodynamically controlled.

In addition to the self-assembly of tethers on surfaces, there has recently been substantial computational studies of the organization of colloidal NPs to which are grafted a finite number of tethers [36–41]. Polymer-tethered spherical nanoparticles have been studied using both SCFT [42,43] and polymer reference interaction site model (PRISM) theory [44–46]. Zhang *et al.* introduced a computational framework in which solvent conditions lead to the immiscibility of NPs and tethers resulting highly ordered phases similar to those found in block copolymers and liquid crystals [36]. Anisotropic interactions due to particle shape and tether location play an important role in the assembly of these structures with spherical [47–51], cubic [41,52], rodlike [38,39,49,53,54], V-shaped [55], and more complex shaped nanoparticles [36]with tethers arranged in a variety of configurations. In addition to the assembly of equilibrium structures, this framework has predicted a route toward dynamic reconfigurability between helical structures through solvent quality switchability [56].

The systems described above can all be described by the following characteristics:

(1) The formation of a given thermodynamic macrostate occurs via minimization of the free energy $F=E-TS$, where E is the internal energy, T is the temperature, and S is the entropy associated with the macrostate.

(2) The entropy can be broken into two parts consisting of (a) a configurational component S_{config} that describes how the set of all tethers is distributed throughout space and (b) a conformational component S_{conform} that describes the various shapes each tether adopts.

It is standard to employ computational methods such as Monte Carlo (MC), molecular dynamics (MD), and dissipative particle dynamics (DPD) in predicting equilibrium self-assembled phases in these systems. These techniques sample, in different ways, the phase space accessible to a system with the system eventually evolving to the global free energy minimum if kinetic traps are avoided. Since these techniques are limited to calculating the energy and not the free energy, it is difficult to know if the system has evolved to the stable global minimum or whether it is trapped in a kinetically arrested state that is only a local free energy minimum. Fur-

*Corresponding author; sglotzer@umich.edu

thermore, these simulations often take hundreds to thousands of hours of computational time because of the large number of states that must be sampled [5].

To circumvent these limitations, we seek a new method able to calculate the free energy of a tethered system directly. As a first step toward this goal, we coarse grain over the tether conformations and replace them with an effective entropic interaction. Our coarse-graining procedure will be similar to the method used in converting an Ising model to a ϕ^4 field theory in that, in both cases, we obtain an effective entropic interaction as part of a phenomenological free energy. Rather than replacing a collection of Ising spins with a continuous field, we will be replacing the many individual beads of a tether with a single bead located at the binding site. This coarse-grained bead will possess an effective entropy that contributes to the total system free energy.

In the limit that the conformational entropy is much greater than the configurational entropy,

$$F = E - TS_{\text{conform}}, \tag{1}$$

is a good estimate for the free energy of the system. Since tethers are flexible, the number of conformations accessible to them may greatly outnumber the configurations they can sample. As such, this approximation is expected to work well for highly flexible tether systems, such as the linear organic chains like those described above. This method of approximating the free energy provides two benefits. First, it allows one to calculate *ex post facto* the change in the free energy for systems whose configurational entropy is negligible. Second, if F can be computed reasonably quickly, then one can rapidly determine the stable states of the system by running a Metropolis MC simulation on the coarse-grained system with the degeneracy Ω that arises from the coarse graining appearing as a prefactor to the Boltzmann factor. This degeneracy can be absorbed into the exponent of the Boltzmann factor as $S=k_BT \ln \Omega$, where S is the entropy associated with the coarse graining. This is equivalent to replacing the energy in the Boltzmann factor with the free energy.

This paper is organized as follows. In the next section, we describe in detail the mathematics behind our coarse-graining scheme. In Sec. III, we consider the case where the tethers are assumed to be noninteracting. In Sec. IV, we approximate the entropic interaction between tethers as a simple two-body potential. In Sec. V, we examine how well the two-body approximation holds for tethers grafted at one end to planar surfaces. In Sec. VI, we use Metropolis MC and our coarse-grained model to simulate the phase separation of tethers on a planar surface and compare with previously published results. In the final section, we discuss the implications of our results.

II. EXACT FORMULATION OF THE CONFORMATIONAL ENTROPY OF TETHERS

The system we consider consists of N tethers bound to a surface of arbitrary geometry. Each tether's attachment point on the surface is free to move so that configuration of tethers on the surface may change over time. We define tethers of type i to be composed of L_i beads each of radius σ_i. Each bead is bound a distance $2\sigma_i$ away from its neighbors in the chain and no beads may overlap. No other restrictions are placed on a tether's conformations. In this analysis, we confine the tethers' binding locations to lattice sites for simplicity without loss of generality. Nearest-neighbor tethers interact with energy $-\xi$ if they are of the same type and zero otherwise. The total energy of the system depends solely on its configuration without regard to individual tether conformations.

Consider a single tether bound to some site x on a surface with a specified geometry. We define $\Omega_{x,i}$ as the number of conformations tether i can assume without allowing any of its beads to overlap with either the system surface or another bead in i. On a flat, cylindrical, or spherical surface, $\Omega_{x,i}=\Omega_i$ is identical for all sites in the system. In contrast, all sites are not identical for tethers bound to corrugated or faceted surfaces. (For tethers bound to small, mobile. interacting colloidal particles, sites can be treated as either identical or nonidentical depending on whether one treats the colloid as a surface or as part of the tether.) For a system in which tether beads can move in continuum space, $\Omega_{x,i}$ will not be finite. This will be of little consequence, however, since we are concerned only with changes in the entropy and calculations of ΔS require only knowledge of the ratio of the number of obtainable states.

We define the avoidance probability $p(i \otimes \{k\})$ as the probability that tether i will not intersect any other tethers in the set $\{k\}$ in its local vicinity. Here, the local vicinity is defined to be the maximum range over which tethers can overlap. It should be emphasized that $\{k\}$ is a set of mutually avoiding tethers. The avoidance probability is useful to obtain since its determination allows one to compute the conformational entropy of tether i directly and therefore to calculate the free energy change of the system. Given $p(i \otimes \{k\})$, one easily obtains the conformational entropy of tether i,

$$S_i = k_B \ln[\Omega_{x,i} p(i \otimes \{k\})], \tag{2}$$

where $k_B=8.617\times10^{-5}$ eV/K is Boltzmann's constant, and the total conformational entropy of the system is given by

$$S = \sum_{i=0}^{N-1} S_i. \tag{3}$$

We are not typically interested in the absolute magnitude of the entropy but rather its change in going from one state to another. To compute the change in the entropy that occurs when tether i moves from site y with a local configuration of tethers $\{j\}$ to another site x with a local configuration of tethers $\{k\}$, we have

$$\frac{\Delta S_i}{k_B} = \ln[\Omega_{x,i} p(i \otimes \{k\})] - \ln[\Omega_{y,i} p(i \otimes \{j\})] = \ln\left[\frac{\Omega_{x,i} p(i \otimes \{k\})}{\Omega_{y,i} p(i \otimes \{j\})}\right] = \ln\left[\frac{\Omega_{x,i}}{\Omega_{y,i}}\right] + \ln\left[\frac{p(i \otimes \{k\})}{p(i \otimes \{j\})}\right]. \tag{4}$$

As can be seen, we need not compute the exact value for $\Omega_{x,i}$ since only the ratio matters. For systems in which $\Omega_{x,i}$ is identical at all sites, this ratio will cancel. In computing ΔS_i,

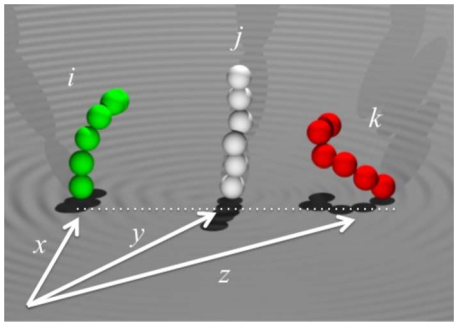

FIG. 1. (Color online) Three tethers i, j, and k with $L_i=L_j=L_k=6$ located along a line at positions x, y, and z, respectively.

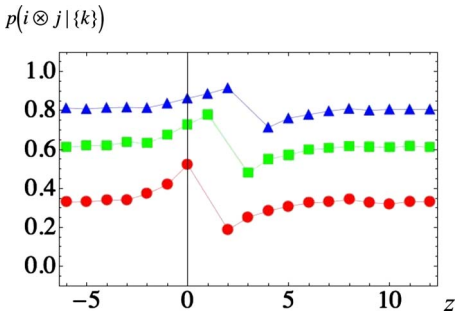

FIG. 2. (Color online) Plots of $p(i\otimes j|k)$ vs z for $x=0$ and $y=1$ (red, circle), 2 (green, square), and 3 (blue, triangle). This data was obtained from 10 000 trials with tethers of length $L_i=6$ beads each of radius $\sigma_i=0.5$.

which can be determined from the configuration only, we have now effectively coarse-grained out any information about the tethers' conformations. It is worth stressing that this entropy is the conformational entropy only and does not contain any contributions by the configurational entropy. Configurational states can be sampled directly by using Metropolis MC to rearrange the tethers' binding sites, as one would rearrange the locations of spins in an Ising model. Sampling states in this way will increase the computational speed since one is not simultaneously sampling the many conformational microstates of the tethers. The tradeoff is that one must now compute the entropy so that it may be included in the free energy term found in the Boltzmann factor.

To compute the entropy, one must compute $p(i\otimes\{k\})$. This avoidance probability cannot be calculated in any trivial way because the interaction between tethers is statistically a many-body interaction. For this reason, we must resort to numerical methods to obtain $p(i\otimes\{k\})$. Before describing how one can compute $p(i\otimes\{k\})$ numerically, it is illustrative to show exactly why the effective entropic interaction between tethers is a many-body one. Consider a system of three tethers arranged on a line as shown in Fig. 1. What is the probability $p(i\otimes j|k)$ that tether i located at x avoids tether j located at y given the presence of a third tether k located at z that does not overlap with j? We computed $p(i\otimes j|k)$ using MC in the following way. First, randomly generated self- and mutually avoiding tethers j and k were created and placed at positions y and z, respectively. Next, a self-avoiding tether i was generated and placed at x. If i did not overlap j, the trial was recorded as a successful attempt. This procedure was repeated 10^4 times and the probability of a successful attempt was calculated. A plot of $p(i\otimes j|k)$ as a function of z for several values of y is given in Fig. 2. The probability of i avoiding j increases as j moves away from i as one would expect. However, the presence of k, which j must avoid, affects j's probability density, shifting it either toward or away from i depending on the location of k. This shift results in either an increase or decrease in $p(i\otimes j|k)$. As this simple example illustrates, the interaction between two tethers depends not only on the distance between them but also on the configuration of tethers around them, making the interaction, by definition, a many-body interaction.

The many-body avoidance probability $p(i\otimes\{k\})$ can be calculated using MC integration in the following way. First, generate the desired configuration of tethers in set $\{k\}$ in any conformation that satisfies the constraint that all tethers must be mutually avoiding. On a flat surface, one can choose this first set of tether conformations such that all beads in a given tether are arranged along a line perpendicular to the surface. Second, choose a tether in set $\{k\}$ and replace its conformation with a randomly generated conformation. If the tether beads in this new conformation do not overlap with any other beads belonging to tethers in $\{k\}$, keep the new conformation; if not, repeat this step until a nonoverlapping conformation is chosen. Repeat this procedure until all members of set $\{k\}$ are replaced resulting in an entirely new conformation for all tethers in $\{k\}$. Next, generate a new conformation for tether i. If tether i avoids all tethers in set $\{k\}$, then the resulting structure is recorded as a successful attempt. Repeat this procedure beginning with the first step and calculate the fraction of successful attempts at nonoverlapping configurations. This fraction will approach the $p(i\otimes\{k\})$ in the limit that the number of trials goes to infinity.

In general, this method of computing $p(i\otimes\{k\})$ will be time consuming for systems with long or densely packed tethers because most newly generated conformations will overlap with other tethers in the vicinity and many trials will need to be attempted before an acceptable conformation is found. Below, we will consider approximations of $p(i\otimes\{k\})$ that can be computed quickly, but first we consider whether or not one can build a look-up table for the values of $p(i\otimes\{k\})$ obtained for different configurations. Look-up tables can greatly expedite tedious calculations in a simulation. The statistical interaction between tethers arises because adjacent tethers share a region of free volume and shift their probability densities to accommodate neighbors. However, even for densely packed surfaces, it is reasonable to expect that two tethers spaced a great distance apart are unlikely to interact. To compute a typical range R for this interaction, we construct $N=(2R+1)^2$ identical tethers consisting of $L_i=5$ beads each of radius $\sigma_i=0.25$ into a hexagonal lattice in which nearest-neighbor binding sites are a distance $a=1$ apart. Using the method described above, we compute $p(i\otimes\{k\})$ as a function of the range R over which the tethers extend as shown in Fig. 3. As can be seen, after a range $R=5$ adding more tethers does not significantly alter $p(i\otimes\{k\})$.

The value obtained above for the range R is prohibitively large. In principle, for a two component (i.e., two types of tether) system of tethers arranged on a hexagonal lattice, one

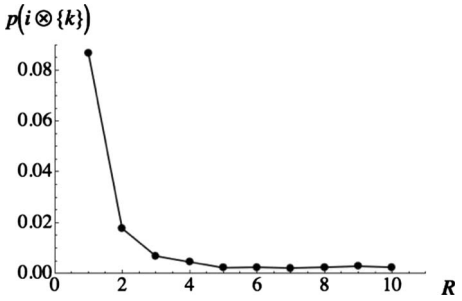

FIG. 3. A plot of $p(i \otimes \{k\})$ vs the range of tethers included in the simulation. This data were obtained from 10 000 trials with tethers of length $L_i=5$ beads each of radius $\sigma_i=0.25$.

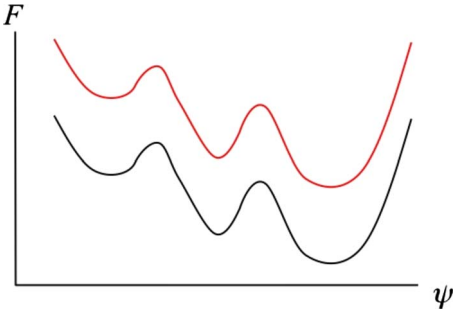

FIG. 4. (Color online) A schematic of the free energy F vs configuration ψ calculated exactly (black) and using some approximate method (red). While there is a large net shift, the relative values of F are constant so that the dynamics obtained by a MC algorithm will be identical in both systems.

could compute a look up table for $p(i \otimes \{k\})$ if the range were nearest-neighbor or next nearest-neighbor since such systems would need at most only $2^7=128$ and $2^{13}=8192$ entries, respectively. However, with a range of $R=5$, one would need 2^{121} entries, vastly more than any computer could compute in the foreseeable future. For this reason, we must employ approximation techniques to compute $p(i \otimes \{k\})$. It should be noted that modifying the values of L_i and σ_i does shift this interaction range, but this shift is not large enough to make a look-up table profitable except in the case of very short or sparsely packed tethers.

Any approximations of $p(i \otimes \{k\})$ must satisfy two criteria: (1) they must allow us to compute reasonably accurately the change in free energy associated with going from one state to another, and (2) they must allow us to compute ΔS_i quickly. The first of these conditions is necessary in order to produce correct results while the latter is a practical consideration that is needed so that one can simulate the system quickly. In addition to these two criteria, it is also desirable to have an approximation scheme that is general enough that it can be applied to a variety of systems. Below, we describe the conditions under which an approximation will meet the first criteria while in the next two sections we describe specific approximation techniques that meet the second criteria and can be applied to a variety of different systems. The results below are presented generally so that they remain true for arbitrary system geometries.

We define $F[\psi]$ as the free energy of a system in some configuration ψ. The free energy can be determined from the internal energy $E[\psi]$, which is purely a function of the system's configuration, and the entropy $S[\psi]$ using

$$F[\psi] = E[\psi] - TS[\psi], \tag{5}$$

We now define $F'[\psi]$ and $S'[\psi]$ to be, respectively, the free energy and entropy computed for the same configuration ψ using some approximation. In general, there will be some deviation between the exact entropy and the approximately computed entropy such that

$$S[\psi] = S'[\psi] + \varepsilon[\psi], \tag{6}$$

where $\varepsilon[\psi]$ is the error in the approximation of the entropy computed for state ψ. This error will generally be different for different configurations. By combining the previous two equations and making use of the fact that the internal energy will be identical in both the approximate and exact cases, we can derive that

$$F[\psi] = F'[\psi] - T\varepsilon[\psi]. \tag{7}$$

In order for an approximation to be valid, it must produce roughly correct values for the change in free energy associated with transitioning between two configurations. We define $\Delta F = F[\xi] - F[\psi]$ as the change in free energy obtained in the transition $\psi \rightarrow \xi$. In order to meet the first criteria listed above, it must be true that

$$\Delta F \approx \Delta F', \tag{8}$$

where $\Delta F'$ is the change in free energy computed using the approximate method. Such a condition will be met if, for all transitions

$$\Delta F \gg T\Delta\varepsilon, \tag{9}$$

or, equivalently,

$$\Delta E - T\Delta S \gg T\Delta\varepsilon, \tag{10}$$

where $\Delta\varepsilon = \varepsilon[\xi] - \varepsilon[\psi]$ is the difference between the approximation errors that arise in the calculation for states ξ and ψ. Since we are concerned with changes in the free energy and not the absolute value of the free energy, it does not matter if our approximation technique systematically overestimates or underestimates $F[\psi]$, so long as it does so consistently for every state. This fact is demonstrated schematically in Fig. 4, which shows an approximation method that exhibits a strong shift in the absolute value of $F[\psi]$ but no change in the relative value of ΔF.

While matching the above criterion is sufficient to show that an approximation is valid, this may not be a necessary condition. In practice, it is difficult to confirm that this criterion will hold for all transitions because of the prohibitively large number of configurations that would need to be tested. Since we are mainly concerned with determining which macrostate is most stable, we can apply a less stringent criterion that is easier to calculate, namely, that Eq. (9) must be true only for transitions between macrostates,

$$\Delta F_M \gg T\Delta\varepsilon_M, \tag{11}$$

where the subscript M denotes that the transition must be from one macrostate to another. The advantage of this criterion is that we still obtain the relative values of free energy between macrostates but we need not test every transition between microstates within the same macrostate. Fluctuations in ε must be small relative to ΔF_M if we are to obtain even qualitatively correct results. However, there is not necessarily a problem if an approximation produces fluctuations in the error that are larger than the fluctuations in a macrostate's free energy because that latter will generally be small. As such, Eq. (11) represents a necessary condition that may also be sufficient if one is concerned only with obtaining the correct macrostate.

To compute $\Delta\varepsilon$, one must first compute $\Delta S'$ and ΔS using the approximate and exact methods, respectively. The change in entropy ΔS can be determined by first computing $\Omega_{x,i}$ and $p(i\otimes\{k\})$ for each state using the MC integration methods described above and then using Eq. (4). We shall define this as the N-body method of computing the entropy. This method, which uses no approximations, will be correct to within numerical precision. In Secs. III and IV, we describe in detail how one can compute $\Delta S'$ for the noninteracting tether and two-body approximations, respectively.

It should be noted that for every approximation made in computing the entropy, there exists some range of parameters where the assumptions hold true. This occurs when the interaction strength, which scales linearly with ΔE, is much greater than k_BT and represents the limit in which demixing occurs. In the opposite limit $k_BT \gg \Delta E$, that the approximation will hold if $\Delta S \gg \Delta\varepsilon$.

III. NONINTERACTING TETHER APPROXIMATION

The above calculation for the entropy change is exact. Unfortunately, $p(i\otimes\{k\})$ is difficult to calculate because of the many-body nature of the statistical interaction between tethers. For this reason, it is advantageous to find approximations for ΔS. The simplest approximation that can be made assumes that tethers do not interact. This assumption will hold for systems in which

$$\ln\left[\frac{\Omega_{x,i}}{\Omega_{y,i}}\right] \gg \ln\left[\frac{p(i\otimes\{k\})}{p(i\otimes\{j\})}\right]. \tag{12}$$

This assumption fails for surfaces that contain identical binding sites since the left hand side of Eq. (12) will be zero. However, when the left hand side is much larger than the contributions due to the interactions between tethers, it will dominate the calculation of the conformational entropy and the interaction terms can be dropped. Intuitively, this assumption is most likely to be valid in systems that have a low density of tethers on the surface and display highly variable surface curvature such as corrugated surfaces or faceted particles. For example, on a tetrahedron, the value of $\Omega_{x,i}$ will depend on whether tether i is bound to a vertex, edge, or face. Under the restriction of Eq. (12), the change in entropy for moving tether i from one site to another can be approximated as

$$\Delta S_i \approx \ln\left|\frac{\Omega_{x,i}}{\Omega_{y,i}}\right|. \tag{13}$$

For systems in which the noninteracting tether approximation is valid, the ratio $\Omega_{x,i}/\Omega_{y,i}$ can be calculated in the following way. For every type of binding site x, generate a random self-avoiding tether configuration bound to the surface at x. Determine whether any of the beads in this tether overlap with any point on the surface. If no beads overlap with the surface, count this configuration as a successful trial. Repeat this procedure many times and compute the probability $p_{x,i}$ that a tether of type i will not overlap the surface when bound at point x. One can then calculate the desired ratio as

$$\frac{\Omega_{x,i}}{\Omega_{y,i}} = \frac{p_{x,i}}{p_{y,i}}. \tag{14}$$

If a surface with variable curvature is densely packed with tethers, then calculating the ratio $\Omega_{x,i}/\Omega_{y,i}$ may not be sufficient because the interaction between tethers and their neighbors may contribute greatly to the conformational entropy. In addition, $p(i\otimes\{k\})$ cannot be easily computed using the simple approximations discussed below because the probability of two tethers overlapping will depend not only on their location but also on the topography of the surface to which they are bound. For these systems, one may be able to approximate the number of conformations accessible to a tether in a way that reflects the presence of other tethers in the system without explicitly including them in the calculation. One such approximation can be obtained by following the same rules described above with one exception. Replace the requirement that tether beads not overlap the surface with the requirement that all beads in tether i must be closer to i's binding site x than to any other binding site. Using this new criterion, one can compute the entropy in a similar way to that described above.

It may be possible to apply these noninteracting tether approximations to faceted and corrugated particles. A complete study of the performance of the above approximations methods in these systems is beyond the scope of this paper but will be included in a subsequent publication. It should be noted that these two noninteracting tether approximations are by no means exhaustive. It may be possible to consider a variety of other mean-field-like approximations that do not explicitly include the interactions between tethers.

IV. TWO-BODY APPROXIMATION

For many surfaces (planes, spheres, cylinders, etc.), each binding site is identical or nearly identical so the noninteracting tether model cannot be employed. For these systems, we need to compute the effective entropic interaction between tethers. Unfortunately, $p(i\otimes\{k\})$ is more difficult to compute than the simple ratios computed in the noninteracting case presented above. The reason for this difficulty is that our approximation method must, of course, satisfy the two basic criteria listed in Sec. II. These two criteria are difficult to implement simultaneously because accurate many-body interactions are inherently slow to compute [57,58]. For this

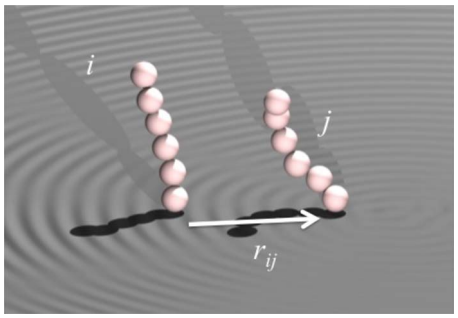

FIG. 5. (Color online) Two tethers i and j separated by some distance r_{ij}.

reason, it is advantageous to consider two-body approximations that produce qualitatively similar results even though this will inevitably sacrifice some accuracy in the calculation.

We seek a general approximation method that will be valid for arbitrary system geometries. With this in mind, we construct our two-body approximation in the following way. Consider two tethers i and j bonded to some surface and separated by some distance r_{ij} as shown in Fig. 5. For the sake of concreteness and simplicity, we will imagine the surface to be planar, although the results are readily generalized to nonplanar surfaces. We approximate the avoidance probability using a two-body potential, by assuming

$$p(i \otimes \{k\}) \approx \prod_{j \in \{k\}} p(i \otimes j), \tag{15}$$

where $p(i \otimes j)$ is the probability that tether i bound at position x avoids tether j bound at position y when no other tethers are in the vicinity. Approximating many-body potentials as two-body interactions is a common semiempirical method [58]. In general, $p(i \otimes j)$ will depend on the number L_i and radius σ_i of the beads. For a planar surface, $p(i \otimes j)$ is purely a function of the scalar distance r_{ij} (or spherical angle θ_{ij} for a spherical surface) between the tethers. For cylindrical, corrugated, faceted, and other surfaces, $p(i \otimes j)$ will depend on the exact locations of i and j rather than just the scalar distance between them.

Using MC, we calculated $p(i \otimes j)$ as a function of the separation between i and j by repeatedly generating two self-avoiding tethers a distance r_{ij} apart and counting the number of times the tethers did not overlap. The results, shown in Fig. 6, are fit with the function

$$p(i \otimes j) = \tanh[m r_{ij} + \phi]/2, \tag{16}$$

which contains two parameters m and ϕ. This functional form was chosen because it has the correct behavior in the $r_{ij} \to \infty$ limit and because it has the expected qualitative shape. More specifically, this functional form reflects the fact that the probability of two tethers avoiding each other decreases sharply after they are brought within a certain distance of each other. In addition, this functional form rapidly approaches one for all separations larger than this distance. Using this fitted function and Eqs. (2), (5), and (15), we can compute $p(i \otimes \{k\})$ and the associated free energies for systems in any configuration. It should be noted that each different combination of tether types in a system, will require its own fitted form for Eq. (16). In the next section, we show that the two-body approximation exhibits qualitative features of the N-body case and use the criteria of Sec. II to determine under what conditions the results are expected to hold.

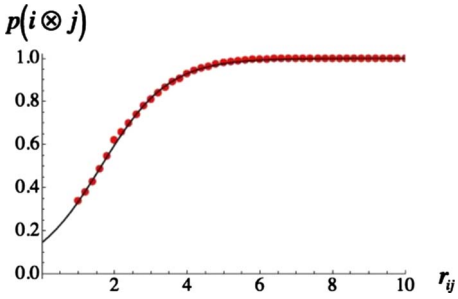

FIG. 6. (Color online) A plot of $p(i \otimes j)$ vs r_{ij} using both data from MC integration (red circles) and the fitted functional form (black line). This data was obtained from 10 000 trials with tethers of length $L_i=6$ beads each of radius $\sigma_i=0.5$. The data were fit to the function form given in Eq. (16) with $m=0.564\,42$ and $\phi=0.973\,32$.

V. COMPARISON OF THE TWO-BODY APPROXIMATION WITH THE EXACT CASE

Before examining whether or not the assumptions made in the two-body approximation fit the criteria listed in Sec. II, it is helpful to first show that they produce qualitatively similar results. To do this, we first construct a $2R+1$ by $2R+1$ hexagonal lattice of tethers of length L_i with beads of radius σ_i. We then compute the value of $p(i \otimes \{k\})$ for this one-component system using the N-body MC integration method described in Sec. II and compare this with the same result computed using the two-body approximation. The results are shown as a function of L_i and σ_i in Figs. 7 and 8, respectively. As can be seen, the plots are qualitatively similar although there is a shift that suggests that the two-body approximation systematically overestimates $p(i \otimes \{k\})$. As stated earlier, a net shift in the entropy should not affect the results so long as the shift is uniform over all states.

Since a net shift in the error will not affect the results, a more appropriate metric with which to gauge the success of

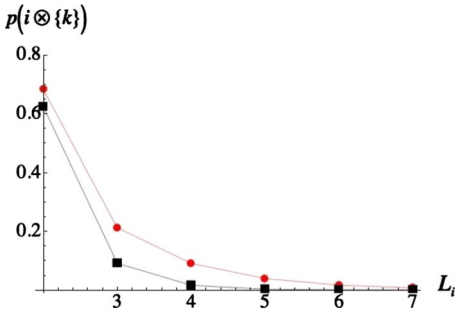

FIG. 7. (Color online) A plot of $p(i \otimes \{k\})$ vs L_i calculated numerically using MC integration (black, square) and using the two-body approximation (red, circle). This data were obtained from 10^4 trials for tether beads of radius $\sigma_i=0.25$ with $R=5$.

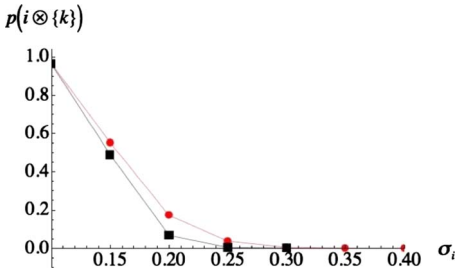

FIG. 8. (Color online) A plot of $p(i \otimes \{k\})$ vs σ_i calculated using the N-body MC integration method (black, square) and using the two-body approximation (red, circle). This data were obtained from 10^4 trials for tethers with $L_i=5$ beads with $R=5$.

the two-body approximation is given by the difference between the errors calculated for different macrostates. If the difference between the errors is much smaller than the change in free energy between these macrostates, then the two-body method may accurately predict the stable state of the system. It is known that DPD simulations of tethers on a planar surface assemble three macrostates: phase separated or demixed (D), stripes (S), and isotropic or mixed (I) [34]. To determine whether or not the two-body approximation holds, we must measure the error for each of these phases.

For each of these three macrostates, we compute the internal energy per particle $E_{M,i}$, the entropy per particle $S_{M,i}$, the two-body approximation of the entropy per particle $S'_{M,i}$, and the error in the approximation $\varepsilon_{M,i}$. The results for both short ($L_i=3$) and long ($L_i=6$) tethers are shown in Fig. 9. For both the N-body and two-body calculations, only the relative value of the entropy can be computed,

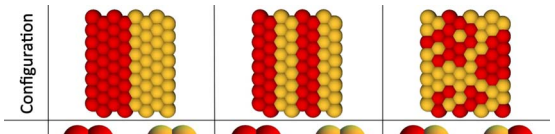

$E_{M,i}$	-3ε		-2ε		$-3\varepsilon/2$	
$S_{M,i}$	-5.95	-2.03	-4.22	-2.64	-4.21	-2.47
$S'_{M,i}$	-3.44	-1.30	-2.72	-1.69	-2.67	-1.73
$\varepsilon_{M,i}$	-2.51	-0.73	-1.50	-0.95	-1.54	-0.74

FIG. 9. (Color online) A chart showing tether configuration and energetic contributions from the D (left), S (middle), and I (right) macrostates. The local configuration around either long (red) or short (yellow) tethers determines the energy per particle $E_{M,i}$ based on the average number of nearest neighbors. For the demixed state, this is computed in the limit that $N \to \infty$ so that the interface and boundaries can be neglected. For simplicity, we only consider stripes of width 2 since they exhibit only one type of local configuration for both tethers. In principle, one could calculate the average energy and entropy per particle for wider stripes, but one must average over multiple local configurations to do so. The N-body and two-body methods are used to compute $S_{M,i}$ and $S'_{M,i}$, respectively. Numerical values of both entropies are given in units of 10^{-4} eV/K. For the isotropic state, the entropy is taken as the average of 100 randomly generated configurations. The error ε is given as the difference between the exact and approximate entropy.

TABLE I. The values of entropy change computed using N-body MC integration and using the two-body approximation for the various transitions.

	$\Delta S_{M,i}$	$\Delta S'_{M,i}$	$\Delta \varepsilon_{M,i}$
D→S	0.56×10^{-4}	0.17×10^{-4}	0.40×10^{-4}
S→I	0.09×10^{-4}	0.01×10^{-4}	0.08×10^{-4}
D→I	0.65×10^{-4}	0.17×10^{-4}	0.48×10^{-4}

$$S_{M,i} = k_B \ln[p(i \otimes \{k\})] \tag{17}$$

and

$$S'_{M,i} = k_B \ln\left[\prod_{j\in\{k\}} p(i \otimes j)\right]. \tag{18}$$

The entropies of the isotropic state were computed by taking the average entropy of 100 randomly generated configurations. In any given macrostate, the magnitude of the error is larger for longer tethers. This is to be expected since larger tethers occupy more free volume, making it more likely that many body effects will play a role. Using the data in this chart, we can calculate the change in the entropy, the two-body approximation for the change in the entropy, and the error for each of the three possible macrostate transitions D→S, S→I, and D→I. The entropy change between macrostates is computed by taking the average value of entropy change for the long and short tethers. The results are shown in Table I. In all cases, difference in the errors $\Delta\varepsilon_{M,i}$ is less than, but on the order of, the change in entropy $\Delta S_{M,i}$ for that transition. For this reason, the two-body approximation is expected to perform well as a toy model at least in the limit that ξ is large; however it is not expected to produce quantitatively accurate results.

Using the data in Fig. 9 and Table I, we compute the change in the free energy between macrostates ΔF_i as a function of ξ for $T=300$ K for each of the three possible transitions. Plots of $\Delta F_i/(T\Delta\varepsilon_i)$ are shown in Fig. 10. The results are expected to be more accurate the further $|\Delta F_i/(T\Delta\varepsilon_i)|$ deviates from unity. In addition to ΔF_i, we use the data of Fig. 9 to compute the free energy F_i of each of the three macrostates as a function of ξ using both the N-body and two-body methods (Fig. 11). For both plots, each macrostate has a region where it has a lower free energy than the other

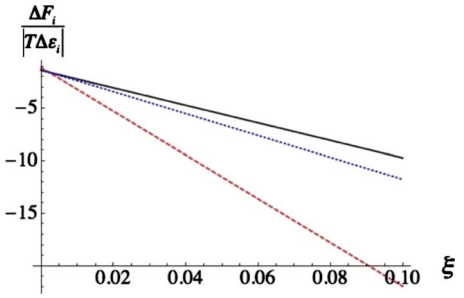

FIG. 10. (Color online) Plots of the free energy $\Delta F_i/(T\Delta\varepsilon_i)$ for macrostate transitions D→I (red, dashed), D→S (blue, dotted), and S→I (black, solid) vs ξ measured in eV.

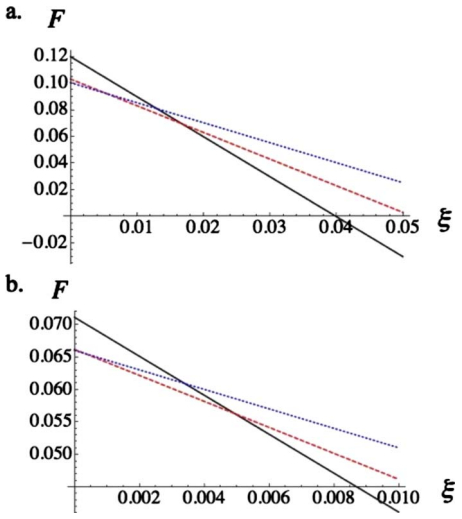

FIG. 11. (Color online) Plots of the free energy F_i vs ξ (measured in eV) for macrostates I (blue, dotted), S (red, dashed), and D (black, solid) computed (a) using N-body MC integration and (b) using the two-body approximation.

two. These results are qualitatively similar both to each other and to what one would expect based on the phase diagram calculated using DPD simulations. Quantitatively, the value at which the transition occurs is strongly shifted. This is not cause for alarm since our model is not expected to give quantitatively precise results.

VI. MODEL SYSTEM: PHASE SEPARATION OF UNEQUAL LENGTH TETHERS GRAFTED ON PLANAR SURFACES

As mentioned earlier, phase separation in a mixture of two types of tethers grafted to planar surfaces were studied earlier using DPD [5,34] and three macrostates—D, S, and I—were identified. It was found that (1) when the two types of tethers are immiscible but equal in length, D is obtained; (2) for a sufficient length difference between the tethers, as ξ increases, the transition from I to S to D occurs. Also, within the striped phase, wider stripes are formed for larger ξ; and (3) when the length difference is increased while keeping ξ constant, stripes become narrower. We now use our simple toy model to simulate this system of tethers of different lengths on a flat surface and test if it can reproduce these three qualitative findings.

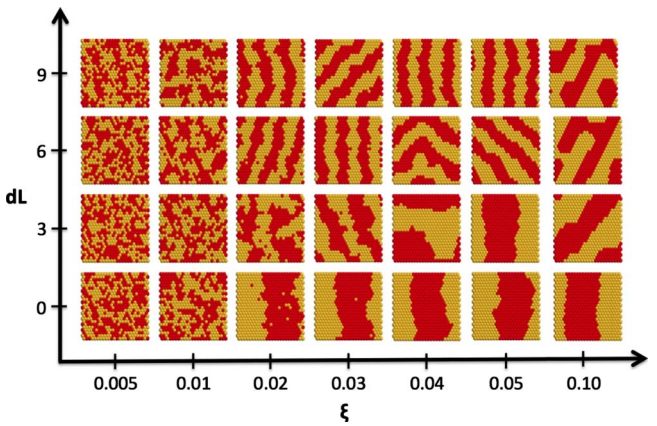

FIG. 12. (Color online) System configurations obtained as a function of tether length difference dL and strength of attraction ξ. As observed in DPD and atomistic simulations [5], stripes are observed for sufficiently large dL provided ξ is not too large.

Since the substrate is flat and $\Omega_{x,i}$ is identical for each lattice site, we use the two-body approximation instead of the noninteracting tether approximation. The systems of tethers simulated along with the parameters m and ϕ for Eq. (16) along with the interaction range, R, are listed in Table II. These parameters were used in MC simulations of 576 (288 of each type) tethers grafted on a flat surface in a hexagonal lattice of unit spacing. The phase-separated equilibrium patterns obtained after 5000 time steps are shown in Fig. 11.

Comparing with the DPD simulations of Singh *et al.* [34], we find good qualitative agreement between the results from our model and DPD. When lengths of the two types of tethers are equal (L_i=3 for both tethers), D phase is obtained expect when ξ is very small and entropy clearly dominates. On increasing length difference, we see that the S phase starts to appear. Stripe width increases as ξ increases and decreases as length difference increases. For very small ξ, the I phase is always formed while for very large ξ we always obtain the expected D phase.

Our model is simulated in a manner similar to a two-dimensional long-range Ising model. For this reason, the CPU time needed to compute the interaction of one tether with all of its neighbors grows as the range of interaction squared. Rigorously speaking, two tethers can interact if their separation is less than the sum of their lengths L. Practically, one can truncate the range of interaction at a value much smaller than this since $p(i \otimes j) \sim 1$ for large separations

TABLE II. Fitted values for the potential.

Length of short tether	Length of long tether	m	φ	R
3	3	0.866442	1.05877	5.0
3	6	0.680911	0.935448	7.0
3	9	0.59626	0.850085	7.0
3	12	0.537607	0.777153	9.0
6	6	0.56442	0.907332	8.0
9	9	0.412497	0.788928	9.0
12	12	0.346807	0.760833	12.0

as can be seen in Fig. 6. Taking this range as an upper bound, the CPU time will grow as $\sim L^2$. A tether can more accurately be viewed as a self-avoiding random walk (SAW). Since the root mean square (RMS) displacement of a SAW grows more quickly than the RMS displacement of a random walk (RW), a RW can be used to compute a lower bound for the CPU time. The range over which two tethers interact should grow as the sum of their RMS displacements. For equal length tethers, the range grows as $\sim\sqrt{L}$ for a RW. For this range, the CPU time needed to compute all the interactions with a tether will grow as $\sim L$. From these bounds, we can state that the CPU time needed will grow as $\sim L^a$, where $1<a<2$. In situations where the algorithm is expected to be slow (e.g., for very long tethers or near critical points), it should be possible to use a biasing scheme just as one would in a long-range Ising model.

The results above confirm the ability of our method to qualitatively incorporate conformational entropy contributions in phase transitions of tether systems. The method can be easily extended to tethers grafted to spherical, cylindrical, or corrugated surfaces and faceted nanoparticles. These geometries will be studied in future publications.

VII. CONCLUSIONS

In this paper, we have presented a coarse-grained model of a system of tethers grafted at one end to a surface of arbitrary geometry. In order to coarse-grain out information about tether conformations, one must replace the information lost with an effective entropic interaction between tethers that will appear in the free energy. If one can find a suitable approximation, then it is possible to compute the conformational entropy of the system. If the conformational entropy is much larger than the configurational entropy, than one can compute approximate values of the free energy and use them to determine whether or not a state is a free energy minimum.

In addition to describing the mathematics behind coarse-graining tether systems, we have presented several simple approximation methods that can be used for various systems. These methods represent only a small fraction of the potential approximations that can be made for tether systems. While more precise approximations can certainly be found, the two-body approximation represents a particularly desirable choice since it is fast to compute and can be easily applied to a number of different systems. Using Metropolis MC simulations on system of tethers bound to a planar surface, we have demonstrated that this two-body method can quickly provide results that are qualitatively similar to those found by non-coarse-grained systems run with DPD. In contrast to DPD, which can take hundreds to thousands of hours of CPU time [5], the coarse-grained tethers system can generally find free energy minimum states in under a few hours.

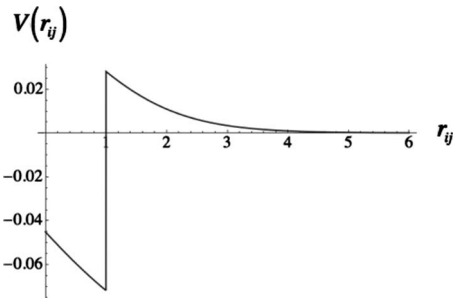

FIG. 13. A plot of the effective interaction $V(r_{ij})$ vs separation distance r_{ij} obtained for $\xi=0.2$, $m=0.660$, and $\phi=0.998$.

It is enlightening to compare our description of the interaction between polymeric chains with that of other researchers. While the toy model method we propose here lacks the elegance of SCFT, PRISM, and other theoretical methods, it is conceptually simpler and readily generalized to other tether systems. To the best of our knowledge, no one has yet applied the theories mentioned above to the self-assembly of polymer tethers on nanoparticles of arbitrary shape. It is straightforward to apply our model to systems of arbitrary geometry. However, this simplicity and generalizability necessarily sacrifices some accuracy in the calculation. In principle, one might be able to include three body and higher order corrections in the calculation if necessary, but this will greatly reduce the speed with which one can simulate the system (Fig. 12).

Finally, when entropy is computed for a system of tethers, we gain insight into the role that tethers play in the self-assembly of nanoscale systems. In general, the morphology of an equilibrium state is determined by the competition between energetic and entropic interactions. The winner of this competition is decided by the free energy. Since the phenomenological free energy we compute is treated like a potential energy in the Boltzmann factor, it is of interest to inquire about the shape of this "potential." To see this, we compute the free energy per particle for a system of two particles and plot this effective potential $V(r_{ij})$ between two like tethers as a function of r_{ij} in Fig. 13. As can be seen, the interaction between particles exhibits a short-range attraction (due to the square-well attraction between like tethers) and a long-range repulsion due to the statistical interaction between tethers. In this way, the effective interaction between tethers is similar in some, but not all, respects to Ising [59], electrostatic [60], magnetic [61], block copolymer [62–65], and chemically reactive binary mixtures [66,67], all of which are known to form stripes.

ACKNOWLEDGMENTS

Financial support for this work was provided by the U.S. Department of Energy (Grant No. DE-FG02-02ER46000).

[1] A. Halperin, M. Tirrell, and T. P. Lodge, Adv. Polym. Sci. **100**, 31 (1992).
[2] S. Y. Jiang, Mol. Phys. **100**, 2261 (2002).
[3] M. E. G. Lyons and S. Rebouillat, Int. J. Electrochem. Sc. **4**, 481 (2009).
[4] J. J. Gooding, F. Mearns, W. R. Yang, and J. Q. Liu, Electroanalysis **15**, 81 (2003).
[5] C. Singh, P. K. Ghorai, M. A. Horsch, A. M. Jackson, R. G. Larson, F. Stellacci, and S. C. Glotzer, Phys. Rev. Lett. **99**, 226106 (2007).
[6] Y. Bohbot-Raviv and Z. G. Wang, Phys. Rev. Lett. **85**, 3428 (2000).
[7] A. J. Spakowitz and Z. G. Wang, J. Chem. Phys. **119**, 13113 (2003).
[8] J. H. Cho and Z. G. Wang, Macromolecules **39**, 4576 (2006).
[9] F. Drolet and G. H. Fredrickson, Phys. Rev. Lett. **83**, 4317 (1999).
[10] G. H. Fredrickson, V. Ganesan, and F. Drolet, Macromolecules **35**, 16 (2002).
[11] E. H. Feng, W. B. Lee, and G. H. Fredrickson, Macromolecules **40**, 693 (2007).
[12] A. V. Dobrynin, A. Deshkovski, and M. Rubinstein, Phys. Rev. Lett. **84**, 3101 (2000).
[13] A. V. Dobrynin and M. Rubinstein, Macromolecules **35**, 2754 (2002).
[14] E. J. Sambriski and M. G. Guenza, Phys. Rev. E **76**, 051801 (2007).
[15] E. J. Sambriski, G. Yatsenko, M. A. Nemirovskaya, and M. G. Guenza, J. Chem. Phys. **125**, 234902 (2006).
[16] E. J. Sambriski, G. Yatsenko, M. A. Nemirovskaya, and M. G. Guenza, J. Phys.: Condens. Matter **19**, 205115 (2007).
[17] P. Ziherl and R. D. Kamien, J. Phys. Chem. B **105**, 10147 (2001).
[18] A. M. Jackson, J. W. Myerson, and F. Stellacci, Nature Mater. **3**, 330 (2004).
[19] A. Centrone, Y. Hu, A. M. Jackson, G. Zerbi, and F. Stellacci, Small **3**, 814 (2007).
[20] G. A. DeVries, M. Brunnbauer, Y. Hu, A. M. Jackson, B. Long, B. T. Neltner, O. Uzun, B. H. Wunsch, and F. Stellacci, Science **315**, 358 (2007).
[21] R. P. Carney, G. A. DeVries, C. Dubois, H. Kim, J. Y. Kim, C. Singh, P. K. Ghorai, J. B. Tracy, R. L. Stiles, R. W. Murray, S. C. Glotzer, and F. Stellacci, J. Am. Chem. Soc. **130**, 798 (2008).
[22] C. Singh A. M. Jackson, F. Stellacci, and S. C. Glotzer, J. Am. Chem. Soc. **131**, 16377 (2009).
[23] A. Perro, S. Reculusa, S. Ravaine, E. B. Bourgeat-Lami, and E. Duguet, J. Mater. Chem. **15**, 3745 (2005).
[24] S. Pradhan, L. P. Xu, and S. W. Chen, Adv. Funct. Mater. **17**, 2385 (2007).
[25] S. Jiang, M. J. Schultz, Q. Chen, J. S. Mooret, and S. Granick, Langmuir **24**, 10073 (2008).
[26] R. K. Shah, J. W. Kim, and D. A. Weitz, Adv. Mater. **21**, 1949 (2009).
[27] I. K. Voets, R. Fokkink, T. Hellweg, S. M. King, P. de Waard, A. de Keizer, and M. A. C. Stuart, Soft Matter **5**, 999 (2009).
[28] A. Walther, M. Drechsler, S. Rosenfeldt, L. Harnau, M. Ballauff, V. Abetz, and A. H. E. Muller, J. Am. Chem. Soc. **131**, 4720 (2009).
[29] Y. H. Chen, C. Y. Wang, Y. Li, and Z. Tong, Prog. Chem. **21**, 615 (2009).
[30] K. H. Roh, D. C. Martin, and J. Lahann, Nature Mater. **4**, 759 (2005).
[31] K. H. Roh, M. Yoshida, and J. Lahann, Langmuir **23**, 5683 (2007).
[32] M. Yoshida, K. H. Roh, and J. Lahann, Biomaterials **28**, 2446 (2007).
[33] C. Guarise, F. Manea, G. Zaupa, L. Pasquato, L. J. Prins, and P. Scrimin, J. Pept. Sci. **14**, 174 (2008).
[34] C. Singh, K. Kuwabara, F. Stellacci, and S. Glotzer (unpublished).
[35] J. J. Kuna, K. Voitchovsky, C. Singh, H. Jiang, S. Mwenifumbo, P. K. Ghorai, M. M. Stevens, S. C. Glotzer, and F. Stellacci, Nature Mater. **8**, 837 (2009).
[36] Z. L. Zhang, M. A. Horsch, M. H. Lamm, and S. C. Glotzer, Nano Lett. **3**, 1341 (2003).
[37] M. A. Horsch, Z. L. Zhang, and S. C. Glotzer, Architecture and Application of Biomaterials and Biomolecular Materials **1**, 231 (2004).
[38] M. A. Horsch, Z. L. Zhang, and S. C. Glotzer, Phys. Rev. Lett. **95**, 056105 (2005).
[39] M. A. Horsch, Z. L. Zhang, and S. C. Glotzer, J. Chem. Phys. **125**, 184903 (2006).
[40] E. R. Chan, L. C. Ho, and S. C. Glotzer, J. Chem. Phys. **125**, 064905 (2006).
[41] X. Zhang, Z. L. Zhang, and S. C. Glotzer, Nanotechnology **18**, 115706 (2007).
[42] E. Reister and G. H. Fredrickson, Macromolecules **37**, 4718 (2004).
[43] E. Reister and G. H. Fredrickson, J. Chem. Phys. **123**, 214903 (2005).
[44] A. Jayaraman and K. S. Schweizer, Langmuir **24**, 11119 (2008).
[45] A. Jayaraman and K. S. Schweizer, Macromolecules **41**, 9430 (2008).
[46] A. Jayaraman and K. S. Schweizer, J. Chem. Phys. **128**, 164904 (2008).
[47] C. R. Iacovella, M. A. Horsch, Z. Zhang, and S. C. Glotzer, Langmuir **21**, 9488 (2005).
[48] C. R. Iacovella, A. S. Keys, M. A. Horsch, and S. C. Glotzer, Phys. Rev. E **75**, 040801 (2007).
[49] C. R. Iacovella, M. A. Horsch, and S. C. Glotzer, J. Chem. Phys. **129**, 044902 (2008).
[50] C. R. Iacovella and S. C. Glotzer, Nano Lett. **9**, 1206 (2009).
[51] C. R. Iacovella and S. C. Glotzer, Soft Mater. **5**, 4492 (2009).
[52] E. R. Chan, X. Zhang, C. Y. Lee, M. Neurock, and S. C. Glotzer, Macromolecules **38**, 6168 (2005).
[53] A. J. Crane, F. J. Martinez-Veracoechea, F. A. Escobedo, and E. A. Muller, Soft Matter **4**, 1820 (2008).
[54] M. A. Horsch, Z. Zhang, and S. C. Glotzer, Nano Lett. **6**, 2406 (2006).
[55] T. D. Nguyen, Z. Zhang, and S. C. Glotzer, J. Chem. Phys. **129**, 244903 (2008).
[56] T. D. Nguyen, and S. C. Glotzer, Small **5**, 2092 (2009).
[57] B. M. Axilrod and E. Teller, J. Chem. Phys. **11**, 299 (1943).
[58] J. A. Barker, R. A. Fisher, and R. O. Watts, Mol. Phys. **21**, 657 (1971).
[59] U. Low, V. J. Emery, K. Fabricius, and S. A. Kivelson, Phys. Rev. Lett. **72**, 1918 (1994).
[60] H. M. McConnell, Proc. Natl. Acad. Sci. U.S.A. **86**, 3452

(1989).
[61] C. Roland and R. C. Desai, Phys. Rev. B **42**, 6658 (1990).
[62] F. S. Bates and G. H. Fredrickson, Annu. Rev. Phys. Chem. **41**, 525 (1990).
[63] A. Chakrabarti and J. D. Gunton, Phys. Rev. E **47**, R792 (1993).
[64] A. Chakrabarti, R. Toral, and J. D. Gunton, Phys. Rev. Lett. **63**, 2661 (1989).
[65] Y. Oono and M. Bahiana, Phys. Rev. Lett. **61**, 1109 (1988).
[66] S. C. Glotzer and A. Coniglio, Phys. Rev. E **50**, 4241 (1994).
[67] S. C. Glotzer, D. Stauffer, and N. Jan, Phys. Rev. Lett. **75**, 1675 (1995).